Low radio frequency observations and spectral modelling of the remnant of Supernova 1987A

J. R. Callingham,[1,2,3]★ B. M. Gaensler,[1,3,4] G. Zanardo,[5] L. Staveley-Smith,[3,5]
P. J. Hancock,[3,6] N. Hurley-Walker,[6] M. E. Bell,[2,3] K. S. Dwarakanath,[7]
T. M. O. Franzen,[6] L. Hindson,[8] M. Johnston-Hollitt,[8] A. Kapińska,[3,5] B.-Q. For,[5]
E. Lenc,[1,3] B. McKinley,[3,9] J. Morgan,[6] A. R. Offringa,[3,10] P. Procopio,[3,9]
R. B. Wayth,[3,6] C. Wu[5] and Q. Zheng[8]

[1] *Sydney Institute for Astronomy (SIfA), School of Physics, The University of Sydney, NSW 2006, Australia*
[2] *CSIRO Astronomy and Space Science (CASS), Marsfield, NSW 2122, Australia*
[3] *ARC Centre of Excellence for All-Sky Astrophysics (CAASTRO), Australia*
[4] *Dunlap Institute for Astronomy & Astrophysics, University of Toronto, Toronto, ON M5S 3H4, Canada*
[5] *International Centre for Radio Astronomy Research (ICRAR), The University of Western Australia, Crawley, WA 6009, Australia*
[6] *International Centre for Radio Astronomy Research (ICRAR), Curtin University, Bentley, WA 6102, Australia*
[7] *Raman Research Institute (RRI), Bangalore 560080, India*
[8] *School of Chemical & Physical Sciences, Victoria University of Wellington, Wellington 6140, New Zealand*
[9] *School of Physics, The University of Melbourne, Parkville, VIC 3010, Australia*
[10] *Netherlands Institute for Radio Astronomy (ASTRON), Postbus 2, 2990 AA, Dwingeloo, the Netherlands*

ABSTRACT

We present Murchison Widefield Array observations of the supernova remnant (SNR) 1987A between 72 and 230 MHz, representing the lowest frequency observations of the source to date. This large lever arm in frequency space constrains the properties of the circumstellar medium created by the progenitor of SNR 1987A when it was in its red supergiant phase. As of late 2013, the radio spectrum of SNR 1987A between 72 MHz and 8.64 GHz does not show any deviation from a non-thermal power law with a spectral index of -0.74 ± 0.02. This spectral index is consistent with that derived at higher frequencies, beneath 100 GHz, and with a shock in its adiabatic phase. A spectral turnover due to free–free absorption by the circumstellar medium has to occur below 72 MHz, which places upper limits on the optical depth of ≤ 0.1 at a reference frequency of 72 MHz, emission measure of $\lesssim 13\,000\ \mathrm{cm^{-6}}$ pc, and an electron density of $\lesssim 110\ \mathrm{cm^{-3}}$. This upper limit on the electron density is consistent with the detection of prompt radio emission and models of the X-ray emission from the supernova. The electron density upper limit implies that some hydrodynamic simulations derived a red supergiant mass-loss rate that is too high, or a wind velocity that is too low. The mass-loss rate of $\sim 5 \times 10^{-6}\ \mathrm{M_{\odot}\ yr^{-1}}$ and wind velocity of 10 km s^{-1} obtained from optical observations are consistent with our upper limits, predicting a current turnover frequency due to free–free absorption between 5 and 60 MHz.

Key words: supernovae: individual: SN 1987A – ISM: supernova remnants – radio continuum: general.

1 INTRODUCTION

Supernova 1987A (SN 1987A), discovered in the Large Magellanic Cloud (LMC) on 1987 February 23, was the brightest supernova seen from Earth since the invention of the telescope (Koshiba et al. 1987; Kunkel et al. 1987; Svoboda et al. 1987).

The close proximity of SN 1987A, and the detailed information we have about its progenitor, has meant SN 1987A has played a pivotal role in shaping our understanding of core-collapse supernovae, supernova remnant (SNR) evolution, and the physical properties of the circumstellar medium deposited by a supernova progenitor.

Radio emission from core-collapse supernovae generally occurs when the forward shock sweeps up the dense, slow-moving wind generated by a red supergiant progenitor (Chevalier 1982).

★ E-mail: jcal@physics.usyd.edu.au

However, the progenitor to SN 1987A was very different from those normally associated with radio supernovae. It is believed that SN 1987A's progenitor, Sk−69°202, evolved from a red supergiant into a blue supergiant ∼20 000 years before the supernova event (Crotts & Heathcote 1991; Podsiadlowski, Morris & Ivanova 2007). While the cause of such a transformation is still debated in the literature (e.g. Woosley et al. 1987; Podsiadlowski & Joss 1989; Collins et al. 1999; Smith 2007), this abnormal evolutionary path for a core-collapse supernova progenitor has produced a complex environment which the shock from the supernova event interacts with.

For example, the prompt radio emission detected at 843 MHz by the Molonglo Observatory Synthesis Telescope (Turtle et al. 1987), which faded to an undetectable flux density in under a year (Ball et al. 2001), is understood to be a consequence of the supernova shock interacting with the low-density, fast-moving blue supergiant wind (Storey & Manchester 1987). Radio emission was then re-detected ∼1200 d after the core collapse (Staveley-Smith et al. 1993), indicating that the forward shock of the supernova event was encountering the denser and slower red supergiant wind in the equatorial plane. This interaction produced the radio shell that is now colliding with the clumpy ring observed at optical wavelengths (Crotts, Kunkel & Heathcote 1995; Plait et al. 1995). The hourglass shape of SNR 1987A, formed from the peculiar evolution of the progenitor (Chevalier & Dwarkadas 1995; Sugerman et al. 2005; Potter et al. 2014), also means the forward shock is interacting with hot blue supergiant wind material beyond the termination region at high latitudes (Zanardo et al. 2010). Currently, >9600 d since the supernova event, it is understood that the forward shock has egressed the equatorial ring and is now interacting with the H II and hourglass region, a region formed from the blue supergiant wind expanding into the red supergiant wind (Lundqvist 1999; Potter et al. 2014).

While SNR 1987A has been extensively studied across the electromagnetic spectrum, there have been no observations conducted at low radio frequencies (<0.843 GHz). This was due to SNR 1987A being too low in declination to be observed with Northern hemisphere radio telescopes, and because SN 1987A occurred after all the low radio frequency instruments in the Southern hemisphere were decommissioned, such as the Culgoora circular array (Slee 1995). Low-frequency radio observations of SNRs can constrain the radio spectrum, providing a unique probe for investigating the circumstellar medium via free–free absorption and insights into the shock acceleration process producing the radio emission (e.g. Kassim 1989; Kassim et al. 1995; Lacey et al. 2001; Brogan et al. 2005). Since intrinsic or extrinsic spectral variations are often subtle, low radio frequency observations are an important key in obtaining a large enough lever arm in frequency space to identify any variation. In particular, low radio frequency observations can place constraints on the electron density of the absorbing medium and the mass-loss rate of the progenitor (Chevalier 1982, 1990; Kassim 1989; DeLaney et al. 2014). Considering the forward shock of SNR 1987A has now passed through the densest part of the equatorial ring (Potter et al. 2014; Fransson et al. 2015), low-frequency observations of SNR 1987A can provide mass-loss limits of the progenitor when it was in its red supergiant phase. This is because the detected radio emission from SNR 1987A is dominated by emission from the region between the forward shock, which is propagating into the circumstellar material, and the reverse shock (Chevalier 1982). The temperature and density of the material internal to the reverse shock are such that the radio emission from the interior to the reverse shock is completely absorbed (Chevalier 1982; Lundqvist 1999; Chevalier & Fransson 2003).

In this paper, we present the lowest radio frequency observations of SNR 1987A using the Murchison Widefield Array (MWA; Tingay et al. 2013). The MWA is a low radio frequency aperture array which observed SNR 1987A between 72 and 231 MHz as part of its all-sky survey (Wayth et al. 2015). The observations presented in this paper are over an order of magnitude lower in frequency than the previous lowest frequency observations of SNR 1987A, allowing us to investigate the surrounding circumstellar medium in a part of frequency space previously unobservable. Combined with gigahertz observations from the Australia Telescope Compact Array (ATCA), these observations provide key insights into the interaction of the supernova shock with the circumstellar medium and its properties. The MWA and the ATCA observations, and the relevant data reduction procedures performed, are outlined in detail in Section 2. The resulting radio spectrum and the absorption model fits are described in Section 3. In Section 4, the implications of these model fits on the mass-loss rate and wind velocity of the progenitor of SNR 1987A are discussed.

2 OBSERVATIONS AND DATA REDUCTION

SNR 1987A was observed by the MWA and the ATCA in late 2013 and early 2014. While not simultaneous, the two ATCA observations bracket the MWA observation with an almost equal gap of three months either side. These observations are summarized in Table 1, and the details about the data reduction processes are described below.

2.1 MWA observations and data reduction

SNR 1987A was observed by the MWA between 72 and 231 MHz on 2013 November 8 as part of the GaLactic and Extragalactic All-sky Murchison Widefield Array (GLEAM; Wayth et al. 2015) survey. The GLEAM survey was conducted by observing the sky between declinations of −90° and +25° in a 2 min 'snapshot' mode, utilizing the meridian drift scan technique at seven independent declination settings. SNR 1987A was observed during the drift scan that was centred on a declination of −55°.

The data reduction process that was performed is described in detail by Wayth et al. (2015) and Hurley-Walker et al. (submitted). In summary, COTTER (Offringa et al. 2015) was used to process the raw visibility data from the MWA observations, which involved averaging the data to 1 s time and 40 kHz frequency resolution, and excising radio frequency interference (RFI) using the AOFLAGGER algorithm (Offringa, van de Gronde & Roerdink 2012). An initial model of the sky for the five instantaneous observing bandwidths of 30.72 MHz was produced by observing bright calibrator sources. Hydra A was the calibrator source observed for the declination strip of the survey that included SNR 1987A. Such observations allowed initial amplitude and phase calibration solutions to be applied.

WSCLEAN (Offringa et al. 2014) was used for imaging as it appropriately accounts for wide-field w-term effects. WSCLEAN is a fast generic wide-field imager that uses the w-stacking algorithm (Humphreys & Cornwell 2011) and the w-snapshot algorithm (Cornwell, Voronkov & Humphreys 2012). Since SNR 1987A is unresolved at all MWA observing frequencies, baselines shorter than 60 m were excluded to minimize the contamination of large-scale, diffuse structure present in the LMC, and a u, v-weighting scheme close to uniform weighting was chosen for imaging. In terms of the 'Briggs' scheme, this corresponds to a 'robust' parameter of −1.0 (Briggs 1995). The snapshot observations were imaged across each 30.72 MHz band using multi-frequency synthesis down to the first

Table 1. A summary of the observations of SNR 1987A used in the spectral modelling. Note that ν represents the central frequency of the observing band, S_ν is the total flux density at frequency ν, and ΔS_ν is the uncertainty on the flux density measurement. For the MWA measurements, ΔS_ν is the sum in quadrature of the local rms noise and the systematic uncertainties associated with correcting the deficiencies in the primary beam model. ΔS_ν for the ATCA measurements is the sum in quadrature of the local rms noise and the uncertainties in the gain calibration. a_{PSF} and b_{PSF} are the semi-major and semi-minor axis of the synthesized beam, respectively.

ν (GHz)	S_ν (Jy)	ΔS (Jy)	Epoch	Telescope	a_{PSF} (arcmin)	b_{PSF} (arcmin)
0.076	5.1	0.8	2013 Nov 08	MWA	5.9	5.2
0.084	4.9	0.7	2013 Nov 08	MWA	5.4	4.8
0.092	4.7	0.5	2013 Nov 08	MWA	5.0	4.4
0.099	4.6	0.4	2013 Nov 08	MWA	4.8	4.1
0.107	4.5	0.3	2013 Nov 08	MWA	4.3	3.7
0.115	4.2	0.2	2013 Nov 08	MWA	4.0	3.5
0.123	4.0	0.2	2013 Nov 08	MWA	3.8	3.3
0.130	3.9	0.2	2013 Nov 08	MWA	3.7	3.1
0.143	3.6	0.2	2013 Nov 08	MWA	3.4	2.8
0.150	3.4	0.1	2013 Nov 08	MWA	3.2	2.6
0.158	3.3	0.1	2013 Nov 08	MWA	3.1	2.5
0.166	3.1	0.1	2013 Nov 08	MWA	3.0	2.4
0.174	3.0	0.1	2013 Nov 08	MWA	2.8	2.3
0.181	2.9	0.1	2013 Nov 08	MWA	2.7	2.2
0.189	2.8	0.1	2013 Nov 08	MWA	2.6	2.1
0.197	2.7	0.1	2013 Nov 08	MWA	2.5	2.1
0.204	2.5	0.1	2013 Nov 08	MWA	2.4	2.0
0.212	2.5	0.1	2013 Nov 08	MWA	2.3	1.9
0.219	2.4	0.1	2013 Nov 08	MWA	2.3	1.8
0.227	2.3	0.1	2013 Nov 08	MWA	2.2	1.7
1.375	0.58	0.05	2013 Aug 31	ATCA	0.11	0.09
1.375	0.58	0.04	2014 Feb 04	ATCA	0.08	0.07
2.351	0.43	0.02	2013 Aug 31	ATCA	0.06	0.05
2.351	0.42	0.02	2014 Feb 04	ATCA	0.05	0.04
4.788	0.28	0.01	2013 Aug 31	ATCA	0.03	0.02
4.788	0.30	0.02	2014 Feb 04	ATCA	0.03	0.02
8.642	0.18	0.03	2013 Aug 31	ATCA	0.01	0.01
8.642	0.17	0.02	2014 Feb 04	ATCA	0.01	0.01

negative CLEAN component, without any major cycles. These images then went through a self-calibration loop, using the initial calibration images for quality control and to ensure that the position of sources and the flux density of the image were consistent throughout the process. The rms of the image was then measured and a new CLEAN threshold was set to three times that rms, which was between 200 and 40 mJy for 72–231 MHz, respectively. The observations were then divided into four 7.68 MHz sub-bands and jointly cleaned.

The Molonglo Reference Catalogue (MRC; Large et al. 1981; Large, Cram & Burgess 1991) was used to set an initial flux density scale for the image and to correct for any right ascension-dependent flux density scale errors due to the drift scan technique. An astrometric correction was also performed at this stage to fix bulk ionospheric distortions by using the positions of sources referenced in MRC. The snapshots for the entire observed declination strip were then mosaicked, with each snapshot weighted by the square of the primary beam response.

Finally, the residual declination dependence in the flux density scale, due to uncertainties in the primary beam model, was corrected. This was done by comparing the measured flux density in the mosaics for isolated, unresolved sources above 8σ of the noise floor to that predicted by their radio spectra using the 74 MHz

Very Large Array Low-Frequency Sky Survey Redux (Lane et al. 2014), 408 MHz MRC, and the 1.4 GHz NRAO VLA Sky Survey (Condon et al. 1998). This correction method places the flux density measurements on the Baars et al. (1977) flux density scale and dominates the uncertainty in the flux density measurements. The flux density calibration is accurate to 8 per cent, as assessed by comparing the MWA flux densities at 150 and 230 MHz to the 150 MHz TGSS-ADR1 survey (Intema et al. 2016) and Jansky Very Large Array *P*-band (230–450 MHz) observations of compact, non-variable sources (Hurley-Walker et al., submitted).

We convolved the appropriate synthesized beam at each sub-band frequency to characterize the flux density of all the sources within two degrees of the centre of the LMC for each of the 20 sub-band images. The sub-band image at 200–208 MHz, with SNR 1987A highlighted, is shown in Fig. 1.

The background emission and noise properties of the individual sub-band images were measured using the backgrounding tool Background And Noise Estimator (BANE).[1] BANE defines the background to be the mean of the pixel distribution, and the noise to be the variance about this mean. BANE was designed to quickly and accurately treat some of the unique problems of estimating the background and noise properties of radio images. It utilizes two main techniques to reduce the compute time, whilst retaining a high level of accuracy. First, since radio images can have a high level of correlation between adjacent pixels, BANE calculates the mean and variance on a sparse grid of pixels and then interpolates to give the final background and noise images. Secondly, BANE uses sigma-clipping on the pixel distribution to avoid contamination from source pixels.

BANE calculated the background emission of the MWA images to vary between ~ 0.7 and ~ 0.1 Jy beam^{-1} for 72–231 MHz, respectively. The background and noise properties were then used by the source finding and characterization program AEGEAN v1.9.6 (Hancock et al. 2012) to accurately identify and measure the flux density of the sources in the images. SNR 1987A was unresolved in all the sub-band images, so the flux density measurements were calculated by AEGEAN by fitting a Gaussian, convolved with the synthesized beam, to the source position.

At the lowest four frequencies, the synthesized beam becomes large enough to cause some blending of the Honeycomb nebula (Chu et al. 1995) and a background galaxy (Ball et al. 2001) with SNR 1987A, shown to the south-east of SNR 1987A in the inset of Fig. 1. We estimate the upper limit of the contamination at these frequencies by extrapolating the spectra of the Honeycomb nebula and the background galaxy from a fit above the lowest four frequencies of the MWA data. This results in larger uncertainties for the flux density measurements between 72 and 103 MHz of SNR 1987A.

2.2 ATCA observations and data reduction

SNR 1987A was observed as part of the ongoing ATCA monitoring campaign (project C015, PI: Staveley-Smith) on 2013 August 31 and 2014 February 4 in array configurations 1.5A and 6D, respectively. The observations were conducted using the Compact Array Broadband Backend (CABB; Wilson et al. 2011) system, providing an instantaneous 2 GHz bandwidth, for both linear polarisations, at central frequencies of 2.1, 5.5, and 9.0 GHz. For both observations, PKS B1934−638 was used for gain and bandpass calibration and to set the flux density scale. PKS B0454−810, PKS B0407−658, and PKS B0530−727 were the secondary calibrators used for phase

---

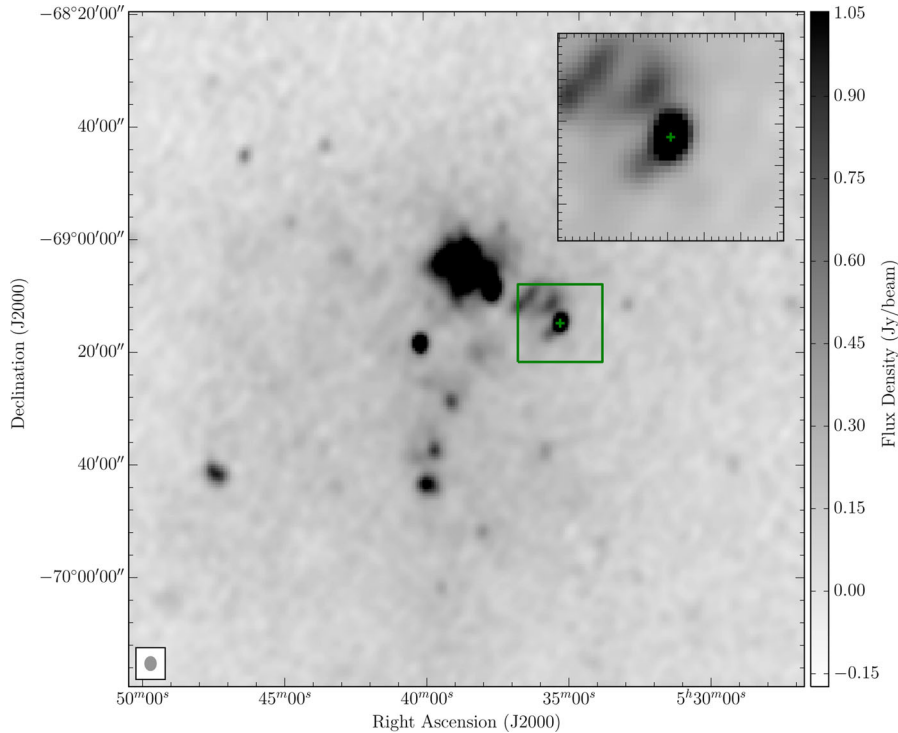[1] https://github.com/PaulHancock/Aegean/wiki/BANE

Figure 1. An MWA image of a part of the LMC at 200–208 MHz formed using a robust weighting parameter of −1 (close to uniform weighting). The position of SNR 1987A is marked by a dark green cross. The inset is a magnified section of the larger image, as represented by the dark green box. The dimensions of the inset are 5.6 arcmin × 5.6 arcmin. In the top left of the inset is the superbubble 30 Doradus C (Mills et al. 1984; Kavanagh et al. 2015), and the source to the south-east of SNR 1987A is a blend of the SNR called the Honeycomb nebula (Chu et al. 1995) and a background galaxy (Ball et al. 2001). The synthesized beam size for this observation is 2.4 arcmin × 2.0 arcmin, and is plotted in the bottom-left corner.

calibration. The total integration time on SNR 1987A in the August and February observations was approximately 7 and 6 h, respectively.

The data reduction process we applied is outlined by Zanardo et al. (2010). In summary, the data for both observations were reduced using the MIRIAD software package (Sault, Teuben & Wright 1995), with known regions of RFI and lower sensitivity in the CABB system initially flagged. The excision of RFI was conducted using the automatic flagging option in `pgflag` and manually with `blflag`. Since the LMC is a crowded field with many bright sources nearby SNR 1987A, only baselines longer than $3\,k\lambda$, where λ is the observing wavelength, were used to form images. To be consistent with pre-CABB monitoring data, the 2 GHz instantaneous bandwidth was split into four sub-bands with 128 MHz bandwidth, centred at 1.4, 2.4, 4.8, and 8.6 GHz. Gain calibration was performed on each sub-band independently. A self-calibration loop was conducted at this stage using a preliminary model generated by CLEANing an image with a small number of iterations, with deeper CLEANing conducted after the self-calibration loop was complete. The flux densities were measured by integrating a Gaussian fit to the emission region at 1.4 and 2.4 GHz, and by integrating over a polygonal region at 4.8 and 8.6 GHz.

3 RESULTS

We present the spectral energy distribution of SNR 1987A from 72 MHz to 8.64 GHz in Fig. 2, plotted using the values reported in Table 1. Applying the Bayesian model inference routine outlined in Callingham et al. (2015), different emission and absorption models were fitted to find the model that best described the spectrum and

to test for any evidence of a spectral turnover or broad spectral curvature. This fitting method assumes that the flux density measurements are Gaussian and the ATCA data points are independent. The known correlation in the MWA flux measurements (Hurley-Walker et al., submitted) was approximated by a Matérn covariance function (Rasmussen & Williams 2006), which produces a stronger correlation between flux density measurements close in frequency space than further away. The Bayesian evidence Z for each fit was calculated using the using the algorithm MULTINEST (Feroz et al. 2013), which is an implementation of nested sampling. Uniform priors for each model parameter in a fit were utilized, allowing direct comparison to least-squares goodness-of-fit tests. While the spectral index of SNR 1987A has been gradually flattening with time (Zanardo et al. 2010), the data were simultaneously fitted since the ATCA observations were almost equally spaced before and after the MWA observation. While the flattening of the spectral index is small over the time between the ATCA and MWA observations (≈0.005), fitting the data simultaneously minimizes any impact of variability.

The physically motivated models investigated included non-thermal synchrotron emission from relativistic electrons at the forward shock front and homogeneous free–free absorption (Mezger & Henderson 1967) caused by the ionized circumstellar material swept up by the shock front. The homogeneous free–free absorption model includes attenuation of the underlying non-thermal synchrotron radiation by an ionized screen internal or external to the emitting electrons. We found the best-fitting model to be the non-thermal synchrotron emission of the form

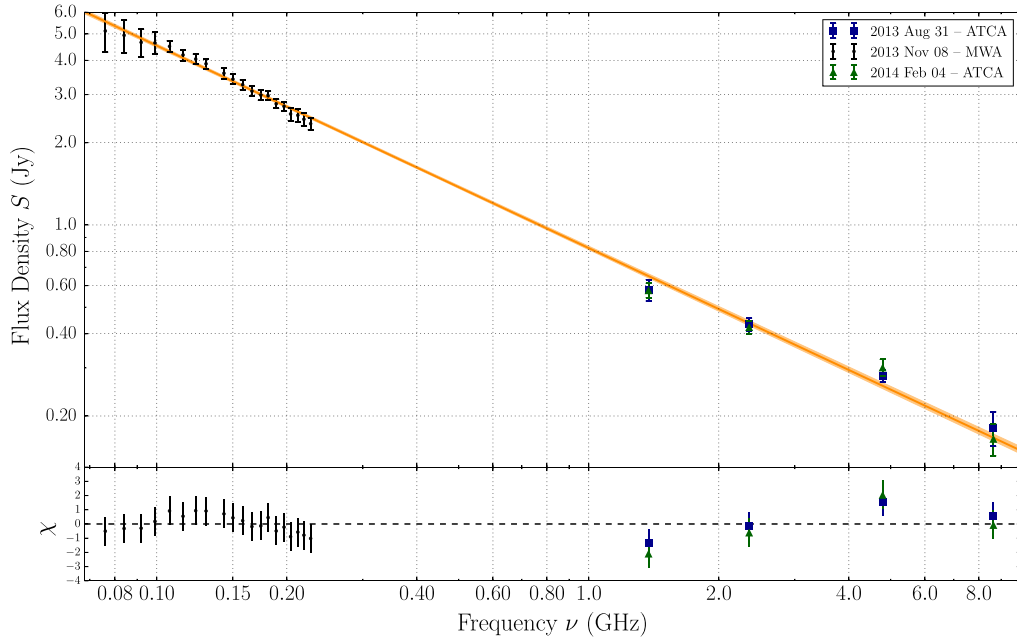$$S_\nu = a \left(\frac{\nu}{1\,\mathrm{GHz}} \right)^\alpha, \tag{1}$$

Figure 2. Spectral energy distribution of SNR 1987A from 0.072 to 8.64 GHz. The MWA data points are plotted in black. The monitoring data from the ATCA for 2013 August 31 and 2014 February 4 are shown in blue and green, respectively. The best-fitting power-law model to all the data is presented in orange, with the shaded orange region representing the 1σ uncertainty on the model fit at the respective frequency. The χ-values for the power-law fit to the data, which represent the residuals to the fit divided by the uncertainties in the flux density measurements, are displayed in the panel below the spectral energy distribution.

where a, in Jy, characterizes the amplitude of the synchrotron spectrum, α is the synchrotron spectral index, and S_ν is the flux density at frequency ν, in GHz. The best fit of this model requires $\alpha = -0.74 \pm 0.02$ and $a = 0.82 \pm 0.01$ Jy. The fit is plotted in Fig. 2 and has a log evidence $\ln(Z)$ value of 8.32 ± 0.02, or a reduced χ^2-value of 0.84, calculated using 25 degrees of freedom. This spectral index is somewhat steeper, but still consistent, with what is expected from the higher frequency ATCA data and leads to a shock compression ratio of $\sigma_s = 3.02 \pm 0.04$, consistent with the range of compression ratios derived for SNR 1987A between 1.4 and 44 GHz (Berezhko & Ksenofontov 2006; Zanardo et al. 2010, 2014). This low compression factor implies that the shock is still in the adiabatic phase and that sub-diffusive shock acceleration, without cosmic ray feedback, is present.

While the spectrum of SNR 1987A is best described by a non-thermal power law, we also fit an extrinsic free–free absorption model to place an upper limit on the optical depth. Assuming that the ionized material is not mixed with the relativistic electrons that are producing the non-thermal spectrum, a spectrum with a peak below 72 MHz is characterized as

$$S_\nu = a \left(\frac{\nu}{0.072\,\mathrm{GHz}} \right)^\alpha \exp\left[-\tau_{72} \left(\frac{\nu}{0.072\,\mathrm{GHz}} \right)^{-2.1} \right], \qquad (2)$$

where τ_{72} is the free–free optical depth at the reference frequency of 72 MHz. The fit to the spectrum requires $\tau_{72} \leq 0.1$ at 3σ.

Model selection can be performed based on the difference between the log evidence of two models $\Delta \ln(Z) = \ln(Z_2) - \ln(Z_1)$, where $\Delta \ln(Z) \geq 3$ is taken as strong evidence that the second model is favoured over the first (Kass & Raftery 1995). The difference in the log evidence value between the free–free absorption fits and synchrotron radiation fit was found to be greater than 200, implying that the non-thermal synchrotron emission is strongly favoured over both internal and external free–free absorption. Non-physically motivated models, such as quadratic and quartic curves, were also

fitted to the spectrum to test for spectral curvature. The difference in evidence between these non-physical models and the synchrotron spectrum was always greater than 165, suggesting that there is no statistical evidence of curvature in the spectrum of SNR 1987A. This implies that if a turnover exists in the spectrum of SNR 1987A, it has to occur at a frequency lower than 72 MHz.

Note that we excluded synchrotron self-absorption as a potential absorption mechanism as it was shown by Chevalier (1998) that synchrotron self-absorption ceased almost immediately after the prompt burst. Additionally, the Razin–Tsytovich effect (Tsytovich 1951; Razin 1957) is unlikely to be contributing to the absorption because it would require the density of the radiating region to be nearly two orders of magnitude larger than the post-shock density, which is greater than expected for the synchrotron emitting region of SNR 1987A (Chevalier 1982; Chevalier & Dwarkadas 1995). Therefore, free–free absorption by an ionized circumstellar material is the only plausible mechanism for a spectral turnover, considering that the observations reported in this paper were conducted over 9640 d since SNR 1987A occurred.

4 DISCUSSION

The MWA observation of SNR 1987A represents the lowest frequency detection of SNR 1987A, over an order of magnitude lower than the previous lowest frequency observations at 843 MHz. This allows us to place a limit on the density of ionized material present around the shock producing the synchrotron emission. Since the best-fitting model is a non-thermal power law, if a turnover is present in the spectrum, it has to occur at or below a frequency of 72 MHz. The medium responsible for the ionized material would likely be the surrounding H II and 'hourglass' regions deposited by the expansion of SNR 1987A progenitor's wind during its red supergiant phase (Chevalier & Dwarkadas 1995). This is because the forward

shock front has swept around the dense equatorial ring $\sim$1000 d before the observations presented in this paper were made (Potter et al. 2014).

Note that our observations are dominated by the emission from the expanding synchrotron emitting shell produced from the interaction of the forward shock with the circumstellar environment (Chevalier 1982). The radio emission interior to this shell is not detected since the density in this region is too low for efficient particle acceleration environments to form, and any emission is absorbed by the dense material that exists between the reverse shock and the interior of the supernova (Lundqvist 1999; Chevalier & Fransson 2003; Potter et al. 2014). Therefore, our observations are only sensitive to absorption by the circumstellar material deposited by the progenitor, rather than intrinsic absorption by the supernova ejecta.

To place an upper limit on the emission measure EM $= \int f n_e^2 \, dl$, we re-parametrize the free–free optical depth from equation (2) in terms of T_e in K, free electron density n_e in cm^{-3}, the path-length l in pc, and filling factor of the ionized gas f as

$$\tau_\nu \approx 8.24 \times 10^{-2} a(T_e, \nu) \nu^{-2.1} T_e^{-1.35} \int f n_e^2 \, dl. \qquad (3)$$

The Gaunt factor $a(T_e, \nu) \approx 1$ for the range of astrophysical quantities investigated in this study (Osterbrock 1989). The form of equation (3) is derived assuming that the H II region is composed of hydrogenic gas, implying an atomic number of ~ 1, and the number density of electrons and ions will be equal since the H II region will be fully ionized from the ultraviolet (UV) radiation emitted from the supernova event. Emission line measurements and environmental simulations suggest that the electron temperature of the H II and 'hourglass' regions will be $\sim 6 \times 10^4$ K after the UV flash (Lundqvist & Fransson 1991; Lundqvist 1999; Sugerman et al. 2005) and before the forward shock of the supernova passes through (Chevalier & Dwarkadas 1995; Potter et al. 2014). Substituting this information, and the fact $\tau_{72} \leq 0.1$, into equation (3) places an upper limit on the emission measure of EM $\lesssim$ 13 000 cm^{-6} pc.

While there is ambiguity about whether the turnover in the spectrum of Galactic SNRs is intrinsic or due to the ionized interstellar medium of the Milky Way (Kassim 1989), the path-length of a photon from SNR 1987A through the interstellar medium of the LMC is significantly shorter than most Galactic SNRs. For example, since the electron density of the LMC near the position of SNR 1987A is measured to be $n_e \sim 0.08$ cm^{-3} (Kim et al. 2003; Cox et al. 2006) and the distance of SNR 1987A from the edge of the LMC is $\sim$1 kpc (Xu, Crotts & Kunkel 1995; Sugerman et al. 2005), the interstellar medium of the LMC has an emission measure EM $\lesssim$ 6 cm^{-6} pc. Hence, any turnover in the spectrum of SNR 1987A would be completely dominated by absorption from material associated with the system of SNR 1987A.

The emission measure also allows us to place an upper limit on the electron density in the red supergiant wind. For a radio photon emitted from the forward shock, it will have an equivalent path-length $l \sim$1 pc, based on the current position of the forward shock and the total size of the H II and 'hourglass' region, assuming that the progenitor was in the red supergiant phase for $\sim$5 $\times$ 10^5 yr (Blondin & Lundqvist 1993; Chevalier & Dwarkadas 1995; Potter et al. 2014). Provided the ionized material is distributed in a slab with a uniform density ($f = 1$), this produces an upper limit on the electron density $n_e = \sqrt{EM/fl} \lesssim 110$ cm^{-3}. While the filling factor of the H II and 'hourglass' region is unknown, any deviation from unity will be small (e.g. Lundqvist 1999; Ohnaka et al. 2008; Fransson et al. 2015), and will have a minimal impact on the electron density limit since dependence on the filling factor goes as $n_e \propto f^{-0.5}$.

An electron density $n_e \lesssim 110$ cm^{-3} is consistent with the limits placed from the detection of the prompt radio emission, as any circumstellar envelope must be relatively thin; otherwise, the prompt radio burst would not have been observed (Storey & Manchester 1987). Such an upper limit on the electron number density is also compatible with models of the X-ray emission from the supernova, which often require a electron density of $n_e \sim 90$ cm^{-3} (Borkowski, Blondin & McCray 1997; Park et al. 2002) in the H II and 'hourglass' region.

We can also estimate the density of the H II and 'hourglass' region from the mass-loss the progenitor underwent when it was a red supergiant. The asymmetric wind profile from Blondin & Lundqvist (1993) has the environmental mass density ρ described in terms of the mass-loss rate of the red supergiant $\dot{M}$, velocity of the red supergiant wind v_w, radius from centre of the system r, and the asymmetry parameter A as

$$\rho(r, \theta) = \frac{3\dot{M}}{(3 - A)4\pi r^2 v_w}(1 - A \cos^2 \theta), \qquad (4)$$

where θ is the angle from the pole of the progenitor. The best-fitting model from the two-dimensional hydrodynamic simulations of Blondin & Lundqvist (1993) found $\dot{M} = 2.0 \times 10^{-5}$ M$_\odot$ yr^{-1}, $v_w = 5$ km s^{-1}, and $A = 0.95$. The asymmetry of the mass-loss produces an equatorial-to-polar density ratio of 20:1. The largest number density of electrons, and thus the most likely site of absorption, will occur just before the forward shock front, which at day 9640 is at $r \sim 0.4$ pc (Potter et al. 2014). In the equatorial plane, this model predicts $n_e \approx 120$ cm^{-3}. This value is close to, but above, the limit we place based on the MWA observations of SNR 1987A.

Therefore, the number density of electrons derived from the model of Blondin & Lundqvist (1993), which is also used by Potter et al. (2014) to model the initial environment of the system, is marginally inconsistent with the upper limit placed by our observations. We note that the inconsistency between the derived and observed electron density is highly dependent on the value of r. To ensure that our findings are robust, we chose a value of r that was at the upper limit of those calculated from the simulations of Potter et al. (2014) and the observations of Zanardo et al. (2014). Since we have used a conservatively large value of r, it is likely either the mass-loss rate is too high and/or the red supergiant wind velocity is too low in the model of Blondin & Lundqvist (1993).

Since the mass-loss rate and wind speed are degenerate, we can parametrize the optical depth in terms of the physical properties of the supernova shock to place a limit on the ratio of the progenitor's mass-loss rate and wind speed. Using the velocity of the forward shock $v_{s,4}$, in units of 10^4 km s^{-1}, and the time since the explosion t_7, in units of 10^7 s, the ratio of the mass-loss rate to velocity of the wind can be expressed as

$$\left(\frac{\dot{M}_{-5}}{v_{w,1}}\right)^2 = 0.25 \nu^2 \tau_\nu (v_{s,4} t_7)^3, \qquad (5)$$

where the mass-loss rate is in units of 10^{-5} M$_\odot$ yr^{-1}, the velocity of the red supergiant wind is in units of 10 km s^{-1}, and the frequency is in units of GHz (Chevalier 1981, 1982). Since the observations reported in this paper were conducted $\approx$ 9640 d since SN 1987A occurred, with $\tau_{72} \leq 0.1$, and $v_s \sim$5000 km s^{-1} (Potter et al. 2014), it follows that $\dot{M}_{-5}/v_{w,1} \leq 2.2$ M$_\odot$ yr^{-1} km^{-1} s. Again, the mass-loss rate and wind velocity derived by Blondin & Lundqvist (1993) are not consistent with our observations. Note that equation (5) may lead to an overestimate of $\dot{M}_{-5}/v_{w,1}$ if the medium is found to be significantly clumpy (Chevalier & Fransson 2003).

Using optical and infrared observations of SNR 1987A, Sugerman et al. (2005) derived a mass-loss rate of $\dot{M} \sim 5 \times 10^{-6}$ M$_\odot$ yr^{-1}, which is close to the median mass-loss rate of the red supergiant population (Knapp & Morris 1985). Additionally, Koo & McKee (1992) suggest a more realistic wind velocity of $v_w = 10$ km s^{-1}, corresponding to a 'slow wind' expanding into a tenuous medium and becoming immediately radiative. Applying either, or both, of these values to equation (5) provides a mass-loss rate-to-wind velocity ratio consistent with our upper limit, and predicts a spectral turnover frequency between ~5 and 60 MHz.

Future observations of SNR 1987A at or below 50 MHz could be helpful in identifying the spectral turnover frequency and providing tighter constraints on the mass-loss rate of the progenitor. The only telescope currently planned that could target SNR 1987A at 50 MHz is the low-frequency array of the Square Kilometre Array (SKA1-Low; Dewdney et al. 2013; de Lera Acedo et al. 2015). However, assuming that equation (4) provides an accurate evolution of the circumstellar medium and that the turnover in the spectrum is currently ~50 MHz, we would predict a turnover frequency of ~10 MHz by the time SKA1-Low becomes operational in approximately 2023. Hence, it is possible that SKA1-Low will not provide better constraints on the spectral turnover than that presented in this paper.

Continual monitoring of SNR 1987A with the MWA will be useful in investigating the physical properties of the circumstellar medium and physics of diffusive shock acceleration. Gradual flattening of the spectral index, in line with higher frequency observations (Zanardo et al. 2010), will provide a more accurate measure of the strength of the magnetic field in the forward shock and the shock compression ratio (Berezhko & Ksenofontov 2006). Additionally, any observed steepening in the spectral index at low radio frequencies, relative to the high-frequency observations, would be indicative of a re-acceleration of electrons by a central compact object (Zanardo et al. 2014). A decrease in the spectral index would suggest the interaction of the shock front with a denser circumstellar medium than currently predicted by mass-loss models of the progenitor.

5 CONCLUSION

We have presented observations of SNR 1987A between 72 MHz and 8.4 GHz, with the MWA observations representing the lowest frequency observations of SNR 1987A to date. This large lever arm in frequency space has allowed us to probe the circumstellar environment of SNR 1987A and test different mass-loss scenarios of the progenitor at an unprecedented level.

The radio spectrum of SNR 1987A does not show any deviation from a non-thermal power law with a spectral index of $\alpha = -0.74 \pm 0.02$. Since free–free absorption has to cause a spectral turnover to occur below 72 MHz, we derived an upper limit on the optical depth $\tau_{72} \leq 0.1$, placing an upper limit on the emission measure of EM $\lesssim 13{,}000$ cm^{-6} pc and electron density of $n_e \lesssim 110$ cm^{-3}. These limits are consistent with limits determined from the detection of the prompt radio emission and X-ray spectra.

The mass-loss rate or wind velocity, or both, derived from the previous hydrodynamic simulations was found to be too high to be consistent with our electron density upper limit. The mass-loss rate of $\dot{M} \sim 5 \times 10^{-6}$ M$_\odot$ yr^{-1} and the wind velocity of $v_w = 10$ km s^{-1}, derived from optical data, are compatible with our observations. Therefore, we predict a current spectral turnover frequency between ~5 and 60 MHz. We conclude that while SKA1-Low will provide lower frequency observations than reported in this paper,

due to the progression of the shock into a lower density circumstellar medium, it will be unlikely that SKA1-Low will detect the spectral turnover once it is operational in approximately 2023.

REFERENCES

Baars J. W. M., Genzel R., Pauliny-Toth I. I. K., Witzel A., 1977, A&A, 61, 99

Ball L., Crawford D. F., Hunstead R. W., Klamer I., McIntyre V. J., 2001, ApJ, 549, 599

Berezhko E. G., Ksenofontov L. T., 2006, ApJ, 650, L59

Blondin J. M., Lundqvist P., 1993, ApJ, 405, 337

Borkowski K. J., Blondin J. M., McCray R., 1997, ApJ, 477, 281

Briggs D. S., 1995, PhD thesis, New Mexico Institute of Mining and Technology

Brogan C. L., Lazio T. J., Kassim N. E., Dyer K. K., 2005, AJ, 130, 148

Callingham J. R. et al., 2015, ApJ, 809, 168

Chevalier R. A., 1981, ApJ, 251, 259

Chevalier R. A., 1982, ApJ, 259, 302

Chevalier R. A., 1990, in Kassim N. E., Weiler K. W., eds, Lecture Notes in Physics, Vol. 362, Low Frequency Astrophysics from Space. Springer-Verlag, Berlin, p. 130

Chevalier R. A., 1998, ApJ, 499, 810

Chevalier R. A., Dwarkadas V. V., 1995, ApJ, 452, L45

Chevalier R. A., Fransson C., 2003, in Weiler K., ed., Lecture Notes in Physics, Vol. 598, Supernovae and Gamma-Ray Bursters. Springer-Verlag, Berlin, p. 171

Chu Y.-H., Dickel J. R., Staveley-Smith L., Osterberg J., Smith R. C., 1995, AJ, 109, 1729

Collins T. J. B., Frank A., Bjorkman J. E., Livio M., 1999, ApJ, 512, 322

Condon J. J., Cotton W. D., Greisen E. W., Yin Q. F., Perley R. A., Taylor G. B., Broderick J. J., 1998, AJ, 115, 1693

Cornwell T. J., Voronkov M. A., Humphreys B., 2012, Proc. SPIE, 8500, 85000L

Cox N. L. J., Cordiner M. A., Cami J., Foing B. H., Sarre P. J., Kaper L., Ehrenfreund P., 2006, A&A, 447, 991

Crotts A. P., Heathcote S. R., 1991, Nature, 350, 683

Crotts A. P. S., Kunkel W. E., Heathcote S. R., 1995, ApJ, 438, 724

de Lera Acedo E., Razavi-Ghods N., Troop N., Drought N., Faulkner A. J., 2015, Exp. Astron., 39, 567

DeLaney T., Kassim N. E., Rudnick L., Perley R. A., 2014, ApJ, 785, 7

Dewdney P. E., Turner W., Millenaar R., McCool R., Lazio J., Cornwell T. J., 2013, SKA-TEL-SKO-DD-001

Feroz F., Hobson M. P., Cameron E., Pettitt A. N., 2013, preprint (arXiv:1306.2144)

Fransson C. et al., 2015, ApJ, 806, L19

Hancock P. J., Murphy T., Gaensler B. M., Hopkins A., Curran J. R., 2012, MNRAS, 422, 1812

Humphreys B., Cornwell T. J., 2011, SKA MEMO 132. Available at: https://www.skatelescope.org/uploaded/59116_132_Memo_Humphreys.pdf

Intema H. T., Jagannathan P., Mooley K. P., Frail D. A., 2016, preprint (arXiv:1603.04368)

Kass R. E., Raftery A. E., 1995, J. Am. Stat. Assoc., 90, 773

Kassim N. E., 1989, ApJ, 347, 915

Kassim N. E., Perley R. A., Dwarakanath K. S., Erickson W. C., 1995, ApJ, 455, L59

Kavanagh P. J., Sasaki M., Bozzetto L. M., Points S. D., Filipović M. D., Maggi P., Haberl F., Crawford E. J., 2015, A&A, 583, A121

Kim S., Staveley-Smith L., Dopita M. A., Sault R. J., Freeman K. C., Lee Y., Chu Y.-H., 2003, ApJS, 148, 473

Knapp G. R., Morris M., 1985, ApJ, 292, 640

Koo B.-C., McKee C. F., 1992, ApJ, 388, 93

Koshiba M. et al., 1987, IAU Circ., 4338

Kunkel W. et al., 1987, IAU Circ., 4316

Lacey C. K., Lazio T. J. W., Kassim N. E., Duric N., Briggs D. S., Dyer K. K., 2001, ApJ, 559, 954

Lane W. M., Cotton W. D., van Velzen S., Clarke T. E., Kassim N. E., Helmboldt J. F., Lazio T. J. W., Cohen A. S., 2014, MNRAS, 440, 327

Large M. I., Mills B. Y., Little A. G., Crawford D. F., Sutton J. M., 1981, MNRAS, 194, 693

Large M. I., Cram L. E., Burgess A. M., 1991, The Observatory, 111, 72

Lundqvist P., 1999, ApJ, 511, 389

Lundqvist P., Fransson C., 1991, ApJ, 380, 575

Mezger P. G., Henderson A. P., 1967, ApJ, 147, 471

Mills B. Y., Turtle A. J., Little A. G., Durdin J. M., 1984, Aust. J. Phys., 37, 321

Offringa A. R., van de Gronde J. J., Roerdink J. B. T. M., 2012, A&A, 539, A95

Offringa A. R. et al., 2014, MNRAS, 444, 606

Offringa A. R. et al., 2015, PASA, 32, 8

Ohnaka K., Driebe T., Hofmann K.-H., Weigelt G., Wittkowski M., 2008, A&A, 484, 371

Osterbrock D. E., 1989, Astrophysics of Gaseous Nebulae and Active Galactic Nuclei. University Science Books, Mill Valley, CA

Park S., Burrows D. N., Garmire G. P., Nousek J. A., McCray R., Michael E., Zhekov S., 2002, ApJ, 567, 314

Plait P. C., Lundqvist P., Chevalier R. A., Kirshner R. P., 1995, ApJ, 439, 730

Podsiadlowski P., Joss P. C., 1989, Nature, 338, 401

Podsiadlowski P., Morris T. S., Ivanova N., 2007, in Immler S., Weiler K., McCray R., eds, AIP Conf. Ser. Vol. 937, Supernova 1987A: 20 Years After: Supernovae and Gamma-Ray Bursters. Am. Inst. Phys., New York, p. 125

Potter T. M., Staveley-Smith L., Reville B., Ng C.-Y., Bicknell G. V., Sutherland R. S., Wagner A. Y., 2014, ApJ, 794, 174

Rasmussen C., Williams C., 2006, Gaussian Processes for Machine Learning. MIT Press, Cambridge, MA

Razin V. A., 1957, Dissertation, Gorkii State University

Sault R. J., Teuben P. J., Wright M. C. H., 1995, in Shaw R. A., Payne H. E., Hayes J. J. E., eds, ASP Conf. Ser. Vol. 77, Astronomical Data Analysis Software and Systems IV. Astron. Soc. Pac., San Francisco, p. 433

Slee O. B., 1995, Aust. J. Phys., 48, 143

Smith N., 2007, AJ, 133, 1034

Staveley-Smith L., Briggs D. S., Rowe A. C. H., Manchester R. N., Reynolds J. E., Tzioumis A. K., Kesteven M. J., 1993, Nature, 366, 136

Storey M. C., Manchester R. N., 1987, Nature, 329, 421

Sugerman B. E. K., Crotts A. P. S., Kunkel W. E., Heathcote S. R., Lawrence S. S., 2005, ApJ, 627, 888

Svoboda R. et al., 1987, IAU Circ., 4340

Tingay S. J. et al., 2013, PASA, 30, 7

Tsytovich V. N., 1951, Vestn. Mosk. Univ., 11, 27

Turtle A. J. et al., 1987, Nature, 327, 38

Wayth R. B. et al., 2015, PASA, 32, 25

Wilson W. E. et al., 2011, MNRAS, 416, 832

Woosley S. E., Pinto P. A., Martin P. G., Weaver T. A., 1987, ApJ, 318, 664

Xu J., Crotts A. P. S., Kunkel W. E., 1995, ApJ, 451, 806

Zanardo G. et al., 2010, ApJ, 710, 1515

Zanardo G. et al., 2014, ApJ, 796, 82

This paper has been typeset from a TEX/LATEX file prepared by the author.